International Journal of Fluid Mechanics Research, Vol. 42, No. 2, 2015

Computational Analysis of Transient non-Newtonian Blood Flow in Magnetic Targeting Drug Delivery in Stenosed Carotid Bifurcation Artery[†]

Haleh Alimohamadi[1], **Mohsen Imani**[2*], and **Behjat Forouzandeh**[2]

[1]Department of Mechanical Engineering,
University of Tehran
Tehran, Iran

[2] School of Electrical and Computer Engineering,
University of Tehran
Tehran, Iran
[*]E-mail: m.imani1386@gmail.com

This paper presents pulsatile blood flow simulation in a carotid bifurcation under the action of external magnetic field. Previous investigations neglected the effect of transient magnetic field on non-Newtonian blood flow through a coupled free and porous media. In this study for closing to a real phenomenon, arterial walls and two fatty deposited atherosclerotic plaques are considered as different porous media, blood is assumed as a generalized non-Newtonian biomagnetic fluid (with Power law and Carreau models) and time dependent inlet velocity varies by the frequency of human heart beating cycle. Because of magnetic field existence, two big vortexes are created at the plaques' edges and the temperature, shear stress, vertical velocity and pressure distribution along the stenosis region have been affected noticeably. The results show by applying $\mathrm{Mn}_F = 10^7$ and $\mathrm{Mn}_M = 10^2$ magnetic field intensity the values of temperature, absolute maximum pressure and shear stress go up $7.35\ \%$, 5.55 times and 5.33 times ($62.16\ \%$,4.08 times and 6 times) respect with normal condition on the upper (lower) plaques respectively. Examining the role of porosity factor indicates that by progressing stenosis disease and hardening atherosclerotic plaques, magnetotherapy treatment lose its efficiency due to sever reduction in available maximum blood temperature, fluid flux and average Nusselt number.

* * *

[†]Received 26.03.2014

ISSN 1064-2277

Nomenclature

$\bar{c}_p$	specific heat $[\mathrm{J}/(\mathrm{kg}\cdot\mathrm{K})]$;
$\bar{\sigma}$	electrical conductivity $[\mathrm{S}/\mathrm{m}]$;
$\bar{\rho}$	density $[\mathrm{kg}/\mathrm{m}^3]$;
$\bar{\chi}_m$	magnetic susceptibility $[\mathrm{m}^3/\mathrm{kg}]$;
$\bar{p}$	pressure $[\mathrm{N}/\mathrm{m}^2]$;
Mn_F	magnetic number (FHD);
$\bar{T}$	temperature [K];
Mn_M	magnetic number (MHD);
T_a	arterial temperature [K];
$\bar{\mu}_0$	magnetic permeability of vacuum $[\mathrm{A}/\mathrm{m}^2]$;
$\bar{k}$	thermal conductivity $[\mathrm{J}/(\mathrm{K}\cdot\mathrm{m}\cdot\mathrm{s})]$;
Pr	Prandtl number;
$\bar{\alpha}$	thermal diffusivity $[\mathrm{m}^2/\mathrm{s}]$;
Da	Darcy number;
$\bar{\eta}$	dynamic viscosity $[\mathrm{kg}/(\mathrm{m}\cdot\mathrm{s})]$;
Re	Reynolds number;
dw	arterial wall thickness;
Ec	Eckert number;
d_o	main vessel radius;
$\bar{u}_i$	inlet velocity $[\mathrm{cm}/\mathrm{s}]$;
dp	plaque thickness;
$\bar{\varepsilon}_p$	porosity of porous media;
$\bar{H}$	magnetic field strength $[\mathrm{A}/\mathrm{m}]$;
$\bar{k}_{br}$	permeability of porous media;
$\bar{B}$	magnetic field induction [Tl];
$\bar{\boldsymbol{V}}(u,v)$	fluid velocity in free region $[\mathrm{m}/\mathrm{s}]$;
$\bar{M}$	magnetization of fluid $[\mathrm{A}/\mathrm{m}]$;
$\bar{\boldsymbol{V}}_p(u_p,v_p)$	fluid velocity in porous region $[\mathrm{m}/\mathrm{s}]$;
$\bar{J}$	density of electrical current $[\mathrm{A}/\mathrm{m}]$;
x, y	component of Cartesian system.

Introduction

Atherosclerotic plaques are implicated to the additional fatty deposits on the inner arterial walls that disturb the normal blood flow in the arteries. The present of these plaques on the purification regions of artery creates more serious situation and unfortunately the arterial trees are more prone to lump formation. The local hemodynamic concept including bifurcation geometry, blood characteristic and properties of arterial walls are discussed in(Friedman et al. [12], Zarins et al. [32]). These models are simulated the blood arteries with rigid walls under the steady-state flow assumption. The other bifurcation models for human arteries with Newtonian blood behavior are brought up in (Bharadvaj et al. [7], Palmen et al. [19], Perktold et al. [20]). The later researches showed that shear rate is significantly high in large arteries while the characteristic of blood flow is not dominant in them(Cho et al. [8], Perktold et al. [20]). Paper (Ku et al. [17]) demonstrates the impact of innate viscoelastic feature of blood flow in 90 degree bifurcation artery and paper (Ley et al. [18]) analyses the characteristic factors such as vessel geometry, plaque size, density and blood flow pattern on the plaques' variation temperature.

Magnetic drug delivery is one of new non-destructive method (Alexiou et al. [2,3]). This procedure can be useful in cardiovascular and articulate diseases (Alimohamadi et al., [4,5]). For example in stenosis artery by usage of magnetic forces we can circulate and concentrate the drug carriers on the target site (Udrea et al. [30]). In order to increase the magnetic field influence on natural blood flow, we can inject some solution Ferro-nanoparticles to it as these particles exert some especial treat under the action of magnetic field. For investigating the behavior of natural blood flow, at first step, biomagnetic fluid dynamics (BFD) has been developed. In mathematical formulation of BFD model only the magnetization impact was taken into account(Haik et al. [16], Tzirtzilakis [28]). New researches show that the electrical conductivity of blood particularly ferrofluid mixture is considerable and for accurate results the Magneto-Hydrodynamic (MHD) influence should be considered (Cramer et al. [9] Sutton et al. [27]). The role of external magnetic field on improving the drug delivery efficiency through the blood vessel networks is studied in (Grief et al. [15]). In (Tzirtzilakis et al. [29]) the velocity and temperature distribution of biofluid flow in a simple rectangular duct under applying the external magnetic field is discussed. This paper considered one dimensional blood flow through a blood artery with solid walls. The transient heat transfer of two-dimensional artery model is brought up in papers (Ai et al. [1]) and (Strek et al. [26]). These papers simulated the blood vessels with rigid walls although in real condition, the artery walls and the formed plaques are porous media. During the last decades, many authors focused on this field and tried to find an accurate coupling model of laminar flow in the free and porous region simultaneously. In article (Rathod et al. [22]) the permeability, magnetic field and body acceleration concepts of stationary blood flow through a porous media are discussed.

The innovation of our paper is solving transient magnetic field and fluid dynamics equations through carotid bifurcation geometry and in coupled free and porous media simultaneously. In our work, the atherosclerotic plaques and the vessel walls have different porosity and two types of common non-Newtonian models (power law and Carreau models) for the blood viscosity is compared with each other. Inflow velocity at the main branch is considered time dependent as a real heart beating and the impact of the magnetic field on different heart cycles is described. In Section 1, the carotid bifurcation geometry and partial differential governing equations on fluid flow in coupled free and porous regions under the influence of magnetic field are developed. Section 2 is dedicated for presenting the dimensionless equations and boundary conditions. Finally, the simulation results are discussed in Section 3 and summarized in Conclusions.

1. Mathematical Formulation

1.1. Geometry description. In this paper the blood flow in carotid bifurcation artery is studied. The modeled artery geometry is taken from (Asakura et al. [6], Perktold et al. [20]) and (Filipović et al. [11]). Carotid artery includes one main branch that the blood enters it and then divides into two bifurcations. Fig. 1 shows this model while on the bigger branch two atherosclerotic plaques are attached to the upper and lower artery walls. The atherosclerotic plaques in addition to the artery walls are considered as porous regions.

This assumption is near to the realistic model because in actual condition the vessel walls and plaques have different porosity features. In this work according to human arterial studies in (Fung [13], Stangeby et al. [25], Wada et al. [31], Zhao et al. [33]), the arterial wall thickness (d_w) and plaque thickness (d_p) are chosen to be 10 and 20 $\%$ of d_o respectively. All the information about branching geometry and values of L_1, L_2 and L_3 is available in [20].

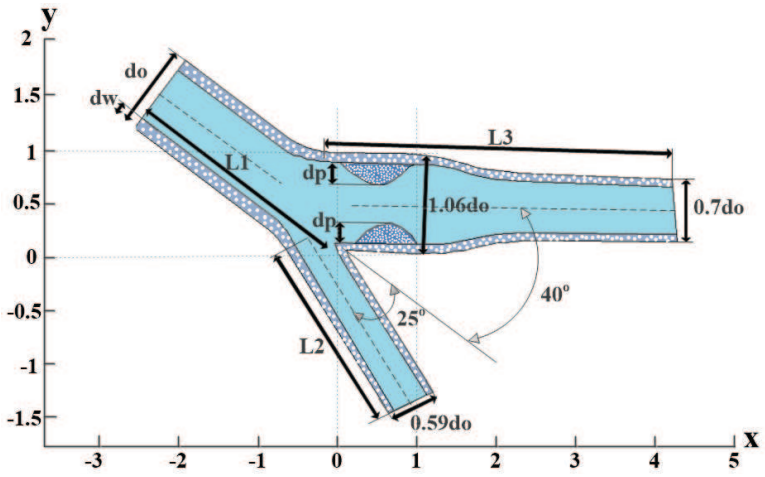

Fig. 1. Artery model (Karl Perktold et al., 1991 [21]).

1.2. Heat transfer and fluid flow equations. The equations describe two dimensional laminar, incompressible, transient, homogenous, non-Newtonian and high electrical conductivity flow in the free and porous regions under the influence of magnetic field consist of extended Navier – Stokes and Brinkman equations.

Free flow.

Continuity equation:

$$\frac{\partial \bar{u}}{\partial \bar{x}} + \frac{\partial \bar{v}}{\partial \bar{y}} = 0. \tag{1}$$

Momentum equation (Tzirtzilakis [28]):

$$\bar{\rho}\left(\frac{\partial \bar{\boldsymbol{V}}}{\partial \bar{t}} + (\bar{\boldsymbol{V}}\cdot\nabla)\bar{\boldsymbol{V}}\right) = -\nabla\bar{p} + \eta\nabla^2\bar{\boldsymbol{V}} + \boldsymbol{F}_L + \boldsymbol{F}_M. \tag{2}$$

Energy equation (Tzirtzilakis [28]):

$$\begin{aligned}&\bar{\rho}\bar{c}_p\left(\frac{\partial \bar{T}}{\partial \bar{t}} + (\nabla\bar{T})\cdot\bar{\boldsymbol{V}}\right) + Q_M - Q_L \\ &\quad = \bar{k}\left(\frac{\partial^2\bar{T}}{\partial\bar{x}^2} + \frac{\partial^2\bar{T}}{\partial\bar{y}^2}\right) + \bar{\eta}\left(2\left(\frac{\partial\bar{u}}{\partial\bar{x}}\right)^2 + 2\left(\frac{\partial\bar{v}}{\partial\bar{y}}\right)^2 + \left(\frac{\partial\bar{v}}{\partial\bar{x}} + \frac{\partial\bar{u}}{\partial\bar{x}}\right)^2\right).\end{aligned} \tag{3}$$

The definition of all the symbols appeared in above equations is included in the Nomenclature.

The additional body forces and heat sources in momentum and energy equations are emerged because of FHD and MHD effect. These terms are calculated by:

$$\begin{aligned}&\boldsymbol{F}_L = \bar{\boldsymbol{J}}\times\bar{\boldsymbol{B}}, \qquad Q_L = \frac{\bar{\boldsymbol{J}}\cdot\bar{\boldsymbol{J}}}{\bar{\sigma}}, \\ &\boldsymbol{F}_M = \bar{\mu}_0\bar{M}\nabla\bar{H}, \qquad Q_M = \bar{\mu}_0\bar{T}\frac{\partial\bar{M}}{\partial\bar{T}}\frac{D\bar{H}}{D\bar{t}}.\end{aligned} \tag{4}$$

In this study for the non-Newtonian blood flow viscosity two common models are compared with each other:

- power law model which is written as below function (Cho et al. [8]):

$$\bar{\eta} = \bar{\eta}_\infty |\dot{\bar{\gamma}}|^m, \tag{5}$$

where $\bar{\eta}_\infty = 0.035$, $m = 0.6$;

- Carreau model (Giannoglou et al. [14]):

$$\bar{\eta} = \bar{\eta}_\infty \left(1 + \frac{\bar{\eta}_0 - \bar{\eta}_\infty}{\bar{\eta}_\infty} \left[1 + \lambda \dot{\bar{\gamma}}\right]^{(n-1)/2}\right), \tag{6}$$

where $\bar{\eta}_\infty = 0.0034$, $\eta_0 = 0.056$, $n = 0.3568$, $\lambda = 3.313$.

Porous region.

The atherosclerotic plaques and blood vessel walls are considered as porous media and slight flow can pass through them. Numerous methods for combining the free and porous flow are suggested. Among them, the Brinkman equations have well precise and eventuate better results. The mass conservation and energy equations for the porous region are similar to the free flow (Eqs. (1) and (3)) but the fluid momentum equation is given by:

$$\frac{\bar{\rho}}{\bar{\varepsilon}_p}\left(\frac{\partial \bar{\boldsymbol{V}}_p}{\partial \bar{t}} + (\bar{\boldsymbol{V}}_p \cdot \nabla)\bar{\boldsymbol{V}}_p\right) = -\nabla \bar{p} + \frac{\bar{\eta}}{\bar{\varepsilon}_p}\left(\frac{\partial^2 \bar{\boldsymbol{V}}_p}{\partial \bar{x}^2} + \frac{\partial^2 \bar{\boldsymbol{V}}_p}{\partial \bar{y}^2}\right) - \frac{\bar{\eta}}{k_{br}}\bar{\boldsymbol{V}}_p + \boldsymbol{F}_L + \boldsymbol{F}_M. \tag{7}$$

The magnetization and Lorentz forces are exerted to the porous regions as well and ε_p and k_{br} are the porosity and permeability of porous regions that are different for the plaques and walls site.

1.3. Magnetic formula. Two horizontal current plates are placed below and upper the stenosis region for circulating flow in the target site and increasing the blood temperature above the plaques' surfaces. The magnetic field is described by the Maxwell law:

$$\begin{aligned} \nabla \times \bar{\boldsymbol{H}} &= \bar{\boldsymbol{J}} = \bar{\sigma}(\bar{\boldsymbol{V}} \times \bar{\boldsymbol{B}}), \\ \nabla \cdot \bar{\boldsymbol{B}} &= \nabla \cdot (\bar{H} + \bar{M}) = 0. \end{aligned} \tag{8}$$

The component of magnetic field intensity for each of current plate along x and y axis are expressed by:

$$\begin{aligned} \bar{H}_x &= -\frac{H_0}{2} \ln \frac{(\bar{x} - \bar{x}_2)^2 + (\bar{y} - \bar{y}_0)^2}{(\bar{x} - \bar{x}_1)^2 + (\bar{y} - \bar{y}_0)^2}, \\ \bar{H}_y &= H_0 \left[\tan^{-1} \frac{\bar{x} - \bar{x}_2}{\bar{y} - \bar{y}_0} - \tan^{-1} \frac{\bar{x} - \bar{x}_1}{\bar{y} - \bar{y}_0}\right], \\ \bar{H} &= \sqrt{\bar{H}_x^2 + \bar{H}_y^2}, \end{aligned} \tag{9}$$

where $\bar{x}_1$, $\bar{x}_2$ and $\bar{y}_0$ are the position of each current plates; H_0 is the magnetic field strength which relays on the applied magnetics induction ($\bar{B} = \bar{\mu}_0(\bar{H} + \bar{M})$. The variation of magnetic field intensity in the whole 2D space is shown in Fig. 2.

As it seen, at the edges of current plates where the magnetic field starts and stops to apply, H_y component varies sharply and could divert blood flow toward the up and down walls; whereas the H_x component is maximize at the middle of plates and pushes the flow backward strongly.

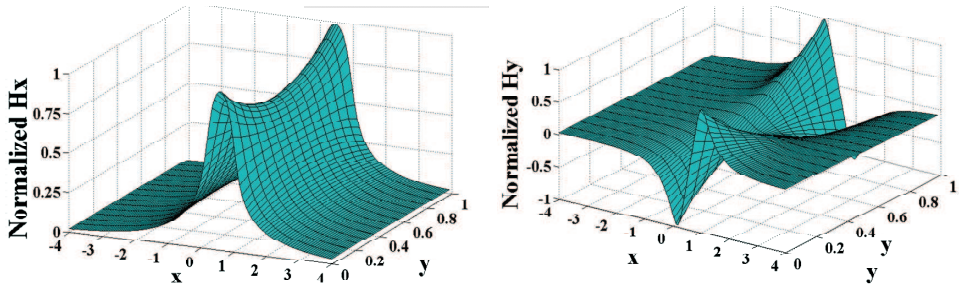

Fig. 2. The components of normalized magnetic field produced by two current plates: a) x-component; b) y-component.

1.4. Magnetization equation. The behavior of blood flow under the action of magnetic field is determined by its magnetization feature. A lot of researches have been done in this field in order to find an appropriate equation. In this study the linear formula that relays on the magnetic field strength and temperature is used(Scarpa et al. [23]):

$$\bar{M} = \bar{\chi}_m \bar{H}. \tag{10}$$

In equilibrium situation the magnetic susceptibility (χ_m) varies with temperature:

$$\bar{\chi}_m = \frac{\chi_0}{1 + \beta(\bar{T} - T_0)}, \tag{11}$$

where χ_0, β and T_0 are constant parameters calculated by experimental researches (Scarpa et al. [23]).

2. Nondimensionalization

In an attempt to find a convenient analysis for this problem the following non-dimensional variables are defined:

$$t = \frac{\bar{\alpha}}{d_o^2}\bar{t}, \qquad x = \frac{\bar{x}}{d_o}, \qquad y = \frac{\bar{y}}{d_o}, \qquad u = \frac{\bar{u}}{u^*},$$
$$v = \frac{\bar{v}}{u^*}, \qquad p = \frac{\bar{p}}{\bar{\rho}u^{*2}}, \qquad H = \frac{\bar{H}}{H_0}, \qquad T = \frac{\bar{T}}{\delta T},$$

where $\bar{\alpha} = \bar{K}/(\bar{\rho}\bar{c}_p)$ is the thermal diffusivity of the fluid and $u^* = \bar{\alpha}/d_o$ is the characteristic velocity. By substituting theses non-dimensional variables into Eqs. (1)−(7) we have in the free flow:

- continuity

$$\frac{\partial u}{\partial x} + \frac{\partial v}{\partial y} = 0; \tag{12}$$

- x-momentum

$$\frac{\partial u}{\partial t} + u\frac{\partial u}{\partial x} + v\frac{\partial u}{\partial y} = -\frac{\partial p}{\partial x} + \mathrm{Pr}|\dot{\gamma}|\left(\frac{\partial^2 u}{\partial x^2} + \frac{\partial^2 u}{\partial y^2}\right) + \mathrm{Mn}_F\chi_m H\frac{\partial H}{\partial x} + \frac{\mathrm{Mn}_M}{\mathrm{Re}}(\chi_m + 1)^2(vH_xH_y - uH_y^2); \tag{13}$$

- y-momentum

$$\frac{\partial v}{\partial t}+u\,\frac{\partial v}{\partial x}+v\,\frac{\partial v}{\partial y}=-\frac{\partial p}{\partial y}+\mathrm{Pr}|\dot{\gamma}|\left(\frac{\partial^2 v}{\partial x^2}+\frac{\partial^2 v}{\partial y^2}\right)$$
$$+\mathrm{Mn}_F\chi_m H\frac{\partial H}{\partial y}+\frac{\mathrm{Mn}_M}{\mathrm{Re}}(\chi_m+1)^2(uH_xH_y-vH_y^2); \tag{14}$$

- energy equation

$$\frac{\partial T}{\partial x}+u\frac{\partial T}{\partial y}+v\frac{\partial T}{\partial y}=\left(\frac{\partial^2 T}{\partial x^2}+\frac{\partial^2 T}{\partial y^2}\right)$$
$$\left[2\left(\frac{\partial u}{\partial x}\right)^2+2\left(\frac{\partial v}{\partial y}\right)^2+\left(\frac{\partial v}{\partial x}+\frac{\partial u}{\partial y}\right)^2\right] \tag{15}$$
$$-\mathrm{Mn}_F\mathrm{Ec}\frac{\partial \chi}{\partial T}H\left(u\frac{\partial H}{\partial x}+v\frac{\partial H}{\partial y}\right)+\frac{\mathrm{Mn}_M}{\mathrm{Re}}\mathrm{Ec}(\chi_m+1)^2(uH_y-vH_x)^2.$$

For the porous region the continuity and energy equations are similar to the free flow but the momentum equations are:

- x-momentum:

$$\frac{\partial u_p}{\partial t}+u_p\frac{\partial u_p}{\partial x}+v_p\frac{\partial u_p}{\partial y}=-\frac{\partial p}{\partial x}+\mathrm{Pr}|\dot{\gamma}|\left(\frac{\partial^2 u_p}{\partial x^2}+\frac{\partial^2 u_p}{\partial y^2}\right)$$
$$+\mathrm{Pr}|\dot{\gamma}|\mathrm{Da}u_p+\mathrm{Mn}_F\chi_m H\frac{\partial H}{\partial x}+\frac{\mathrm{Mn}_M}{\mathrm{Re}}(\chi_m+1)^2(v_pH_xH_y-u_pH_y^2), \tag{16}$$

- y-momentum:

$$\frac{\partial v_p}{\partial t}+u_p\frac{\partial v_p}{\partial x}+v_p\frac{\partial v_p}{\partial y}=-\frac{\partial p}{\partial y}+\mathrm{Pr}|\dot{\gamma}|\left(\frac{\partial^2 v_p}{\partial x^2}+\frac{\partial^2 v_p}{\partial y^2}\right)$$
$$+\mathrm{Pr}|\dot{\gamma}|\mathrm{Da}v_p+\mathrm{Mn}_F\chi_m H\frac{\partial H}{\partial y}+\frac{\mathrm{Mn}_M}{\mathrm{Re}}(\chi_m+1)^2(uH_xH_y-vH_y^2), \tag{17}$$

where

$$|\dot{\gamma}|=\left[2\left(\frac{\partial u}{\partial x}\right)^2+2\left(\frac{\partial v}{\partial y}\right)^2+\left(\frac{\partial u}{\partial y}+\frac{\partial v}{\partial x}\right)^2\right]^{1/2};\qquad \chi_m=\frac{\chi_0}{1+(\beta\delta T)\left(T-\frac{T_0}{\delta T}\right)}.$$

Shear rate norm ($|\dot{\gamma}|$) depends on the non-Newtonian model. For power law model it is

$$|\dot{\gamma}|=\left(\frac{\bar{\alpha}}{d_o^2}\right)^{n-1}\left[2\left(\frac{\partial u}{\partial x}\right)^2+2\left(\frac{\partial v}{\partial y}\right)^2+\left(\frac{\partial u}{\partial y}+\frac{\partial v}{\partial x}\right)^2\right]^{(n-1)/2}, \tag{18}$$

while according to Carreau model,

$$|\dot{\gamma}|=1+\frac{\bar{\eta}_0-\bar{\eta}_\infty}{\bar{\eta}_\infty}\left[1+\left(\frac{\bar{\alpha}}{d_o^2}\lambda\right)^2\left(2\left(\frac{\partial u}{\partial x}\right)^2+2\left(\frac{\partial v}{\partial y}\right)^2+\left(\frac{\partial u}{\partial y}+\frac{\partial v}{\partial x}\right)^2\right)\right]^{(n-1)/2}. \tag{19}$$

The non-dimensional parameters appeared in the written transformed equations are defined, as follows:

$$
\begin{aligned}
&\text{Reynolds number,} && \mathrm{Re} = \frac{d_o \bar{\rho} u^*}{\bar{\eta}_\infty} = \frac{\bar{\rho}\bar{\alpha}}{\bar{\eta}_\infty}\,;\\
&\text{Eckert number,} && \mathrm{Ec} = \frac{u^{*2}}{\bar{c}_p \delta T} = \frac{\bar{\alpha}^2}{\bar{c}_p \delta T d_o}\,;\\
&\text{Prandtl number,} && \mathrm{Pr} = \frac{\bar{\eta}_\infty}{\bar{\rho}\,\bar{\alpha}}\,,\\
&\text{Darcy number,} && \mathrm{Da} = \frac{d_o^2}{\bar{k}_{br}}\,;\\
&\text{Magnetic number of FHD,} && \mathrm{Mn}_F = \frac{\bar{\mu}_0 H_0^2}{\bar{\rho}\, u^{*2}} = \frac{\bar{\mu}_0 H_0^2 d_o^2}{\bar{\rho}\,\bar{\alpha}^2}\,;\\
&\text{Magnetic number of MHD,} && \mathrm{Mn}_M = \frac{\bar{\mu}_0^2 H_0^2 d_o^2 \bar{\sigma}}{\bar{\eta}_\infty}\,.
\end{aligned}
\tag{20}
$$

For boundary conditions, the arterial walls are set at constant temperature (T_a) and base on no slip condition, velocity is zero on them ($u = v = 0$). At the outlet of two branches the gauge pressure is set zero ($p = 0$) and the pressure of other regions are calculated respect to it. It is considered the temperature profile reaches to fully developed condition at the end of each branch such that there is not any temperature gradient at the vessel outlets ($\partial T/\partial n = 0$). The uniform transient velocity at constant temperature (T_a) is entered to the main branch. The velocity is perpendicular to the inlet cross section area and varies with time as Fig. 3 shows (Schelin et al. [24]).

For the free-porous interface, it is assumed that the velocity is equal in these two regions ($\boldsymbol{V}_p = \boldsymbol{V}$). This condition means that the velocity field remains continuous between free and porous media.

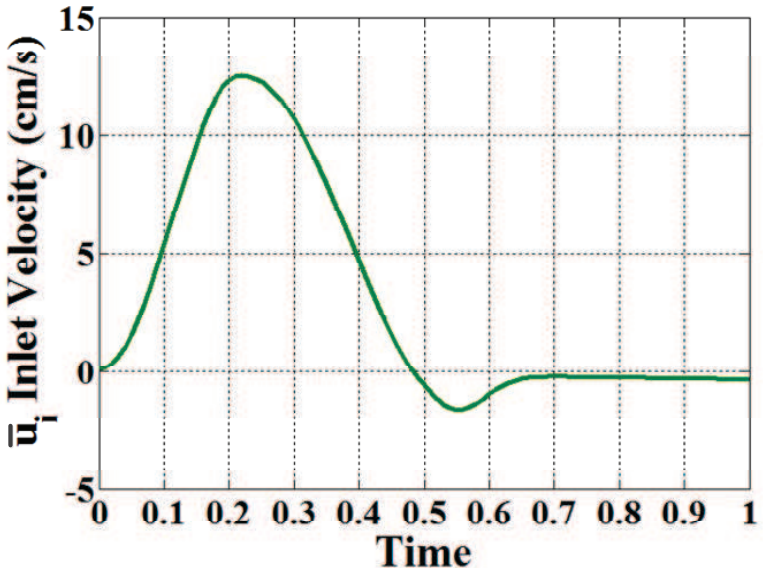

Fig. 3. The inlet velocity $\bar{u}_i$ versus time(Schelin et al., 2012 [24]).

In this paper, the whole of artery domain includes porous and free regions are gridded with unstructured triangle elements. Around plaques and divider wall the mesh distribution is refined. The extra fine mesh including 19000 elements is performed for the carotid bifurcation discrete. For solving Eqs. (12) – (17) with above boundary conditions simultaneously, the multi-physics software package COMSOL is used. This software is based on the finite element method and solves the coupled transient flow in the free and porous regions together. The solution is converged when the relative tolerance controling the error in each integration step become less than 10^{-6} for both velocity and temperature parameters.

3. Simulation Result

The thermophysical and non-dimensional parameters of blood flow, arterial and the plaques used in this paper are archived in Table 1 [10].

The below current plate is located at $x_1 = 0.2$, $x_2 = 1$ and $y_0 = -0.2$ while the upper plate position is $x1 = 0$, $x_2 = 1$ and $y_0 = 1.2$. The constant value that are appeared in the above equations are listed in Table 2 [26].

Table 1.
Physical properties of carotid bifurcation

	Blood	Arterial wall	Plaque
$\bar{\rho}\,[\mathrm{kg/m^3}]$	1050	1075	920
$\bar{k}\,[\mathrm{J/(K \cdot m \cdot s)}]$	$2 \cdot 10^{-3}$	$1.73 \cdot 10^{-3}$	$1.76 \cdot 10^{-3}$
$\bar{c}_p\,[\mathrm{J/(kg \cdot K)}]$	15.9927	12.71	14.86
$\bar{\alpha}\,[\mathrm{J/(kg \cdot K)}]$	$1.191 \cdot 10^{-7}$	$1.265 \cdot 10^{-7}$	$1.287 \cdot 10^{-7}$
Ec	$7.378 \cdot 10^{-6}$	$10.51 \cdot 10^{-6}$	$9.286 \cdot 10^{-6}$
$\mathrm{Pr}_{\mathrm{powerlaw}}$	28.01	25.72	29.55
$\mathrm{Pr}_{\mathrm{carreu}}$	27.61	25.35	29.13
$\mathrm{Re}_{\mathrm{powerlaw}}$	$3.57 \cdot 10^{-2}$	$3.88 \cdot 10^{-2}$	$3.38 \cdot 10^{-2}$
$\mathrm{Re}_{\mathrm{carreu}}$	$3.62 \cdot 10^{-2}$	$3.94 \cdot 10^{-2}$	$3.43 \cdot 10^{-2}$

Table 2.
Used values of the constants

Parameter	Numerical Value
T_a	300 K
δT	30 K
Mn_F	$(10^6 \ldots 10^7)$
Mn_M	$(10^1 \ldots 10^4)$
χ_0	0.06
β	$5.6 \cdot 10^{-3}$ 1/K
$\mathrm{Da}_{\mathrm{plaue}}$	500/1000/1500
$\mathrm{Da}_{\mathrm{walls}}$	100/200/300

3.1. Normal blood flow in carotid bifurcation without magnetic forces. In this paper the length of each blood bifurcation is long enough such that the uniform inlet velocity in the main branch and the flow in the two out flow branches reach to fully developed condition soon. The temperature counter and laminar flow stream lines at the last time ($t = 1$) are shown in Fig. 4. Due to low inlet velocity at the entrance, there is no separated and reversed flow even near the divider wall where the flow divides into two parts and there is high velocity gradient. In the stenosed region, because of the streamlines contraction, the blood velocity magnitude and temperature goes up. In the main branch although the velocity reaches to fully developed condition quickly and the velocity profile is parabolic in each cross section, we face with a thermal entry length problem; such that through the main branch, $3.5\ \%$ increment in the blood temperature than the constant artery walls is distinguishable in Fig. 4. This occurrence is expectable as the Prantdle number is high ($\mathrm{Pr} = 27.6$) and thermal entry length is extremely longer than velocity entry length. All of the below simulation are done with considering Carreau model for biofluid.

The pressure, shear stress, v-velocity and temperature distribution along the lower and upper plaques are shown in Fig. 5. In the stenosis region, the cross sectional area decreases and base on continuity law the flow accelerates and both velocity and temperature magnitude go up. As Fig. 5d elucidates on the both plaques' surfaces the temperature increases at first (about $3.52\ \%$ above the wall temperature) and after that falls down sharply. On the other hand, by accelerating flow, the absolute pressure magnitude declines (as Fig. 5a shows) since the velocity and pressure act vice versa. According to this figure, vertical velocity sign is changed at the approximately middle of each plaque and the upper plaque bears positive shear stress; while, negative shear stress is exerted to the lower plaque (see Fig. 5b).

3.2. Blood flow and heat transfer pattern under the influence of external magnetic field. The stream function and temperature contours at the present of external magnetic field and in three different times steps ($t = 0.4$, 0.5, 0.8) are demonstrated in Fig. 6. The magnetic forces push the fluid flow to the reversed direction and create flow circulation above the plaques' edges. The first vortex rotates clock wise while the second one is counter clock wise. Till $t = 0.4$ the positive inlet velocity prevents vortexes formation in the stenosis region because the viscous and inertia forces acts are highly powerful and disappear the effect of opposite magnetic forces. At $t = 0.4$ the magnitude of these forces (viscous and inertia) dwindle and two vortexes are created in the target site. By passage of the time, these vortexes become stronger and bigger such that they can influence wider area. These vortexes can recirculate the fluid above the plaques and stagnant drug carriers in the target site. Vortex formation concentrates heat transfer in specific locations as the figure shows the blood temperature near the lower and upper plaques increases strongly. In fact, flow recirculation decreases the cooling effect of blood and at $t = 0.9$ the bigger and stronger vortexes not only focuses the maximum temperature on the plaques' surfaces but also increases it approximately 2.07 times higher than simple case without magnetization effect. So, we can conclude the current plate acts as external heat source and rise the fluid temperature locally. This increment is very useful in magneto-therapy method and medical science because some drugs require warm environment for activation and absorption.

3.3. Effect of magnetic field intensity on fluid flow behavior and heat transfer rate. The magnetic field intensity has direct impact on the penetration velocity, temperature, pressure and shear stress. The effect of this parameter on exerted shear stress to upper and lower plaques is demonstrated in Fig. 7. Vortex formation produces negative velocity gradient at the left edge of each plaque and according to the chosen Cartesian system approximately half of the plaques' surfaces tolerate sinistral shear forces. At the middle of each plaque, the sign of shear stress is changed and then increases till its climax. After the peak, shear stress magnitude drops down severely and

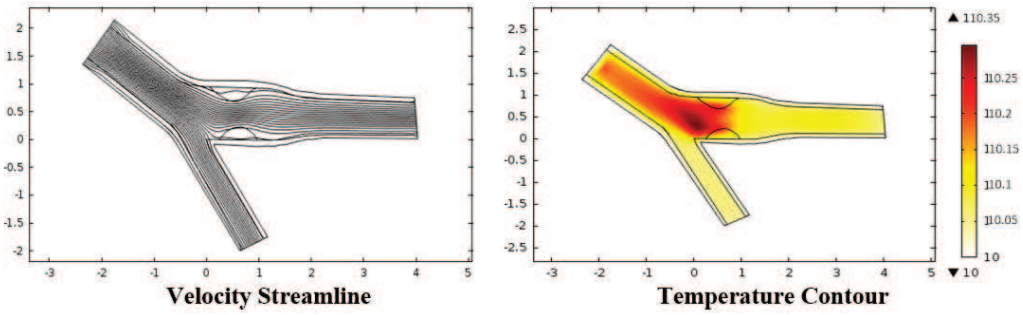

Fig. 4. Velocity streamline and temperature contour without magnetization effect at unit time with $\mathrm{Da}_{\mathrm{plaque}} = 500$, $\mathrm{Da}_{\mathrm{wall}} = 100$.

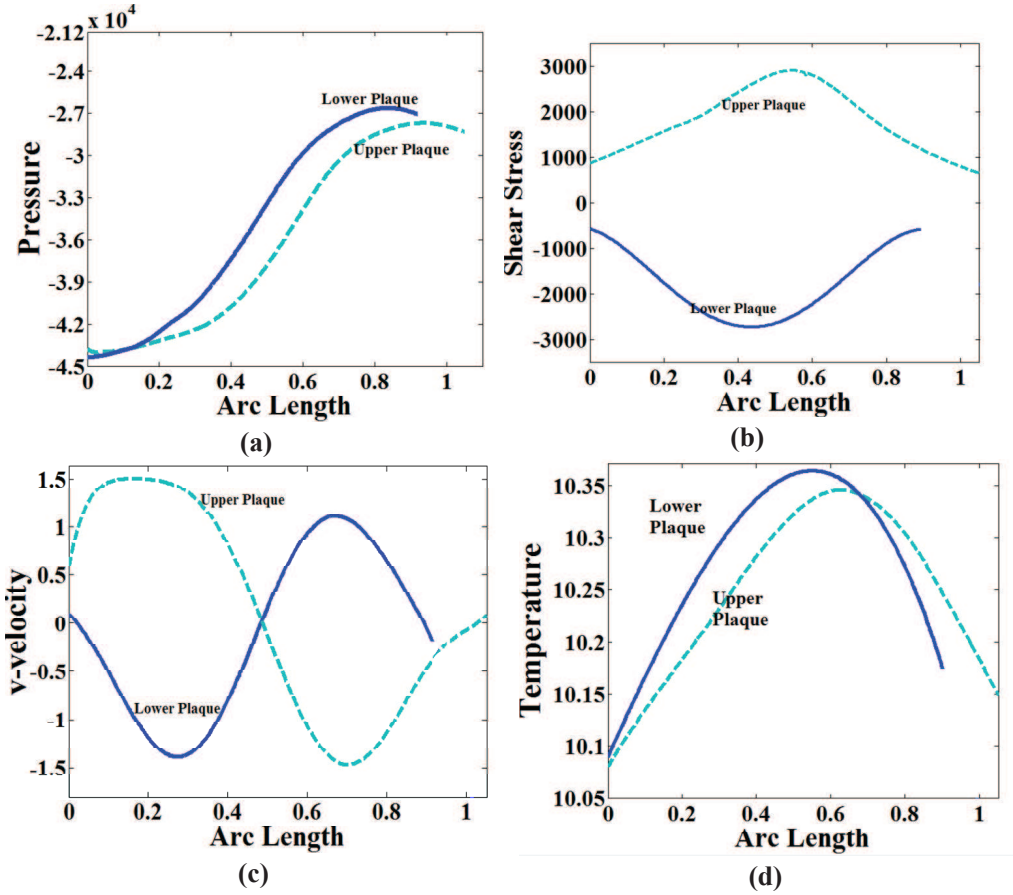

Fig. 5. Field distributions along lower and upper plaques with $\mathrm{Da}_{\mathrm{plaque}} = 500$, $\mathrm{Da}_{\mathrm{wall}} = 100$: a) pressure, b) shear stress, c) v-velocity, d) temperature.

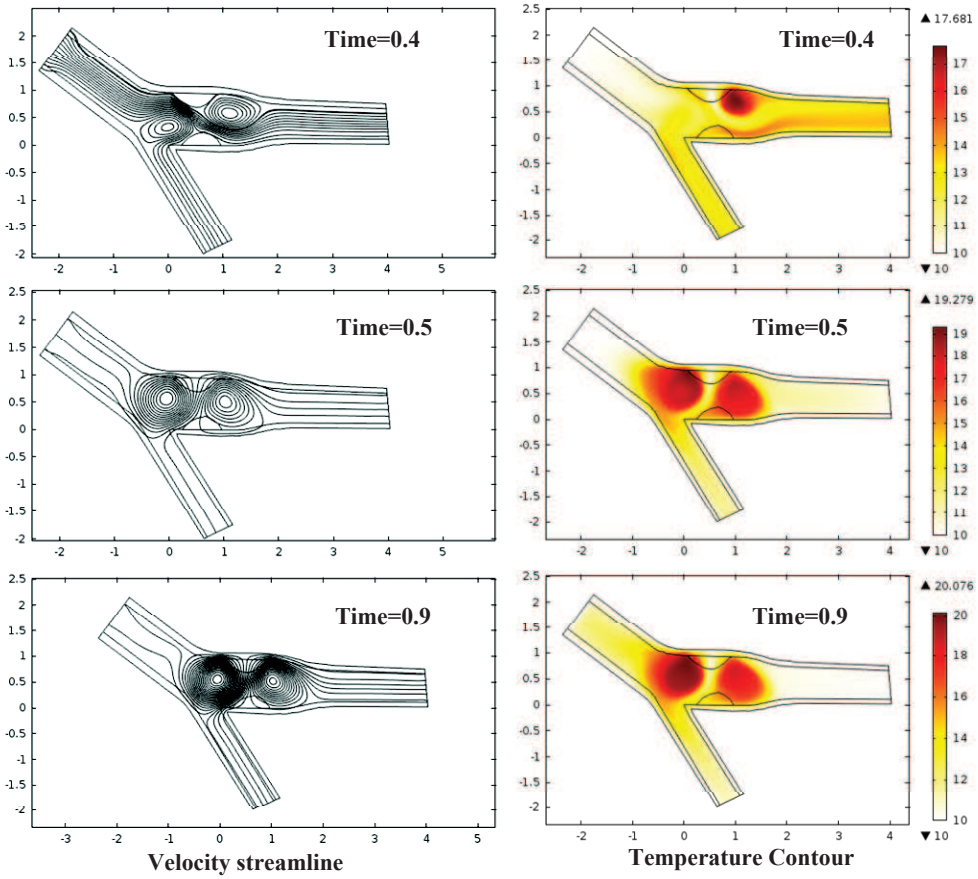

Fig. 6. velocity streamlines and temperature contours in different time step with $\mathrm{Mn}_F = 10^7$, $Mn_M = 10^2$, $\mathrm{Da}_{\mathrm{plaque}} = 500$, $\mathrm{Da}_{\mathrm{wall}} = 100$.

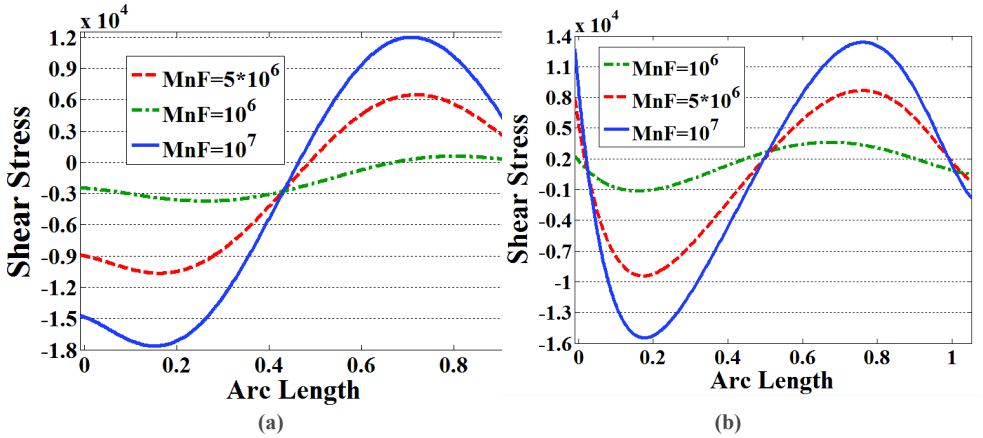

Fig. 7. Shear stress in lower and upper plaques in different magnetization with $\mathrm{Da}_{\mathrm{plaque}} = 500$, $\mathrm{Da}_{\mathrm{wall}} = 100$ and $Mn_M = 10^2$:
a) lower plaque, b) upper plaque.

reaches zero value again because fluid goes out of the vortexes affected domain. Base on the results, by doubling magnetic field intensity from $5 \cdot 10^5$ the maximum shear stress on the lower and upper plaques becomes 1.96 and 1.75 times higher respectively.

Applying magnetic forces and recirculating flow inside the stenosis region result opposite temperature trend on the lower and upper plaques. As Fig. 8 shows the temperature variation along both lower and upper plaques looks like a semi parabolic graph and only has different concavity for these two plaques (in lower plaque concavity is negative and in upper plaque it is positive). Generally, the total surface of plaques experiences higher temperature than the artery walls and this increment relays on the power of external magnetic field. The extremum value of temperature on the lower and upper walls becomes 1.61 and 1.08 times higher due to strengthening the magnetic field intensity from 10^6 to 10^7. Increasing shear stress and temperature along the stenosis region can be useful for cutting or even dissolving the atherosclerotic plaques from the inner side of vessels, as these lumps are usually formed from fatty deposits and are vulnerable to the high temperature and shear stress.

The first noticeable impression of applying magnetic field, as Fig. 9 shows, is negating the vertical velocity along the whole surfaces of atherosclerotic plaques. The negative v-velocity pushes the drug carriers directly into the fatty deposits (lipid) and it is the main target of this paper.

By doubling magnetic field intensity from $5 \cdot 10^5$ the maximum vertical flux into the lower and upper plaques increases about the 6.8 and 8.93 times respectively and this incident is very beneficial for new suggested magnetic drug delivery method. Similar to temperature graphs, vortex formation results opposite pressure distribution on the lower and upper plaques. As Fig. 10 demonstrates on the lower plaque, the pressure goes up until it attains to the maximum value and then declines steeply. On the upper plaque, the pressure decreases as meeting the first left edge of the plaque, this reduction continues till the minimum point and after that the pressure starts to increase. As it is clear in the below figure, applying stronger magnetic forces makes the pressure value positive along the both lumps. This positive pressure can compress the plaques to the wall and make them smaller according to the fact that these lumps are porous region and have good capability for compression. Nowadays, using rigid stents is a common way for treating atherosclerosis. These stents only compress the plaques into the walls and open the vessels lumen. However, due to the probability of vessel rupture, using these stents is dangerous and has high risk of death. New magneto-therapy producers are as effective as embedding stents inside the vessels although they are safer and more efficient.

3.4. The effect of plaques and wall porosity on the magneto-therapy performance. The porous permeability of plaques is another important factor that has direct impact on the efficiency of magneto-therapy. The effect of this parameter on the pressure and temperature distribution along the upper plaque is shown in Fig. 11. As it shown, higher Darcy number makes the magneto-therapy method less efficient because both pressure and temperature magnitudes decrease as far as in some cases the minimum pressure becomes negative. By tripling the Darcy number from 500 to 1500 the minimum temperature declines about 8.11 % and this reduction is not appropriate for our goal. The lower plaque fallows this trend too, as Fig. 12 demonstrates the maximum pressure and temperature on this plaque's surface decline about 10 and 4.76 % respectively. Darcy number also affects the amount of fluid flux into the porous plaques. This impact is shown in Fig. 13 and as it is clear in this figure, increasing permeability of plaques has negative effect on the drug delivery procedure, because by tripling the value of Darcy number, absolute vertical velocity on the lower and upper walls becomes 1.78 and 1.45 times lower respectively.

Variation of maximum temperature and vertical velocity respect with magnetization number (Mn_M) and permeability of artery walls are shown in Fig. 14. In low magnetization number, strengthening the magnetic field intensity does not have suitable results and declines both maximum

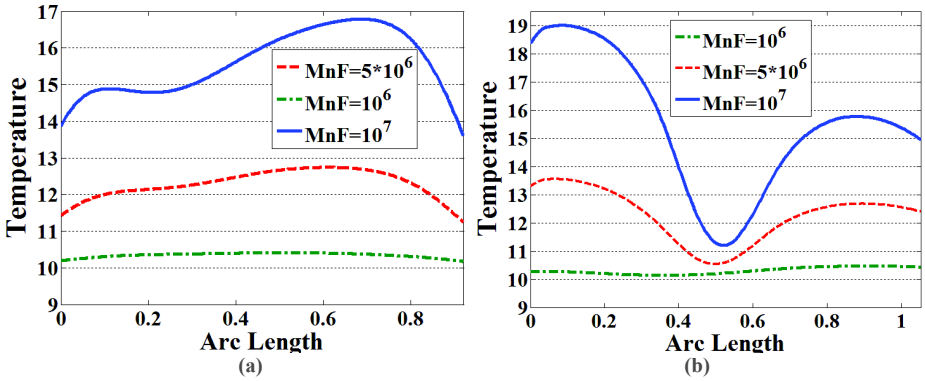

Fig. 8. Temperature distribution in lower and upper plaques in different magnetization with $\mathrm{Da}_{\mathrm{plaque}} = 500$, $\mathrm{Da}_{\mathrm{wall}} = 100$ and $Mn_M = 10^2$:
a) lower plaque, b) upper plaque.

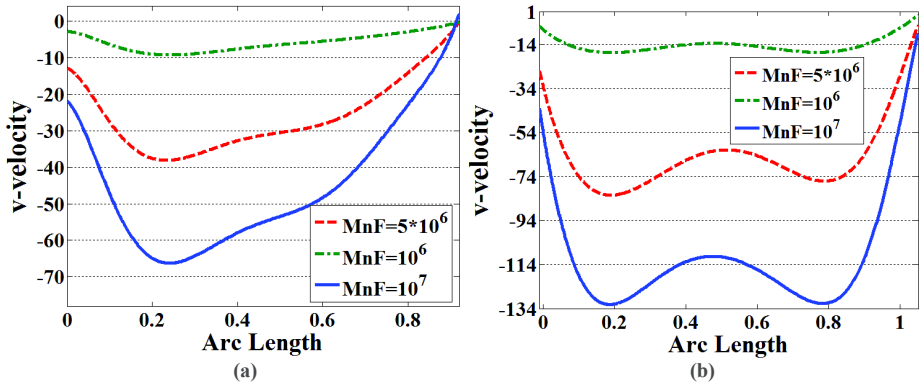

Fig. 9. The v-velocity distribution in lower and upper plaques in different magnetization with $\mathrm{Da}_{\mathrm{plaque}} = 500$, $\mathrm{Da}_{\mathrm{wall}} = 100$ and $Mn_M = 10^2$:
a) lower plaque, b) upper plaque.

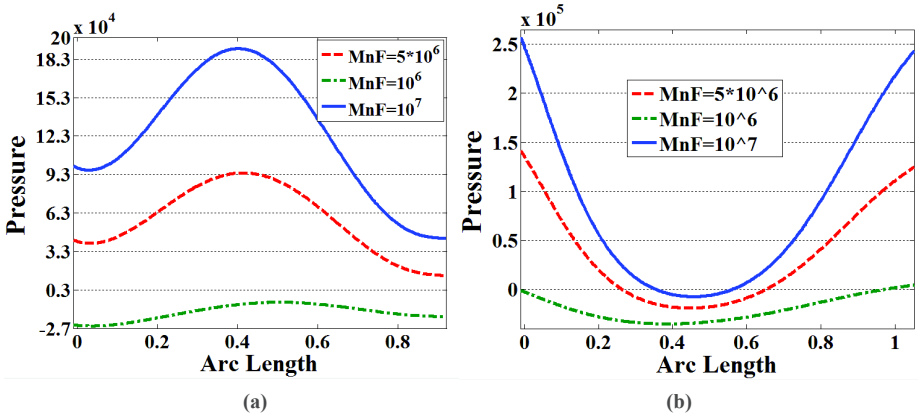

Fig. 10. Pressure distribution in lower and upper plaques in different magnetization with $\mathrm{Da}_{\mathrm{plaque}} = 500$, $\mathrm{Da}_{\mathrm{wall}} = 100$ and $Mn_M = 10^2$:
a) lower plaque, b) upper plaque.

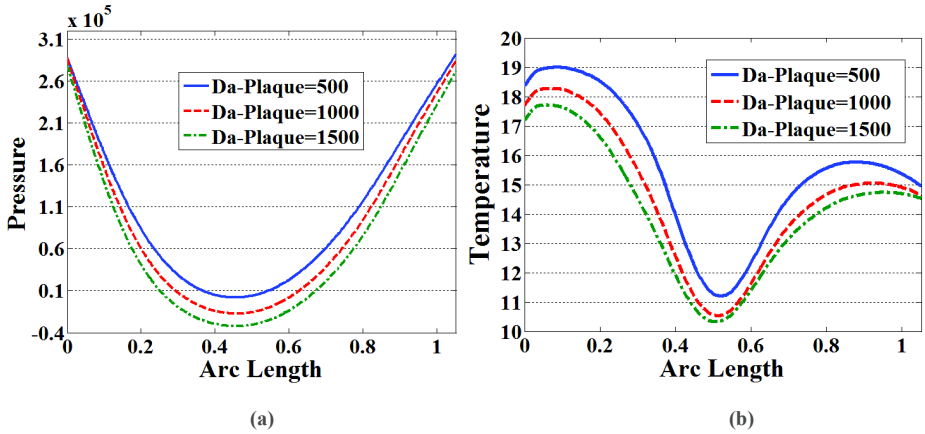

Fig. 11. Field distributions on the upper plaque in different plaque porosity factor with $\mathrm{Mn}_F = 10^7$ and $\mathrm{Mn}_M = 10^2$:
a) pressure, b) temperature.

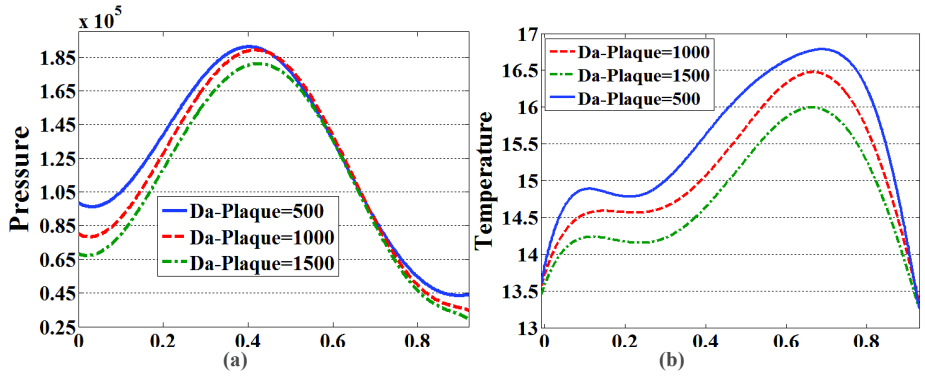

Fig. 12. Field distributions on the lower plaque in different plaque porosity factor with $\mathrm{Mn}_F = 10^7$ and $\mathrm{Mn}_M = 10^2$:
a) pressure, b) temperature.

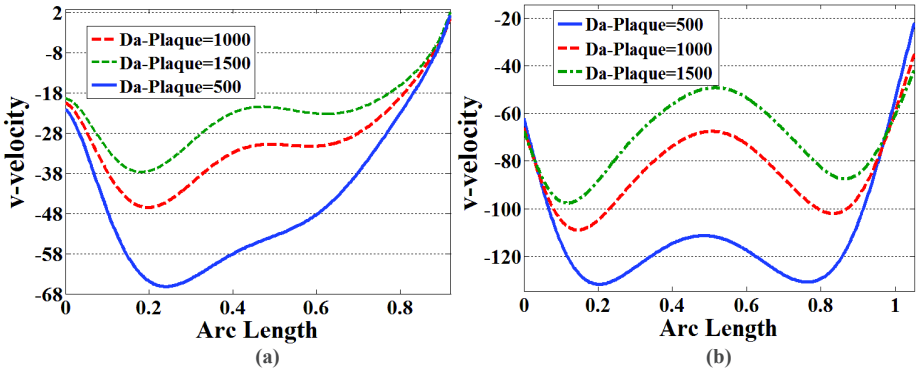

Fig. 13. The v-velocity distribution in different plaque porosity factor with $\mathrm{Mn}_F = 10^7$ and $\mathrm{Mn}_M = 10^2$:
a) lower plaque, b) upper plaque.

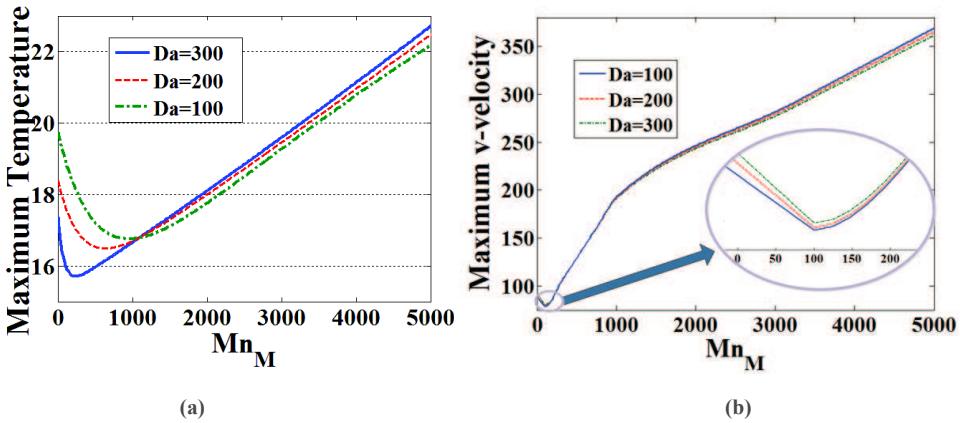

Fig. 14. Variation of maximum values in different walls porosity factor and magnetization number of $\mathrm{Mn}_F = 10^7$: a) for temperature, b) for v-velocity.

temperature and v-velocity. This reduction is justifiable because in low magnetization number, magnetic forces are weak and the fluid is controlled mostly by viscous and inertial forces, so magnetization only decelerates the flow and maximum velocity and consequently the maximum temperature dwindle. After a specific value (Mn_M extremely lower than 10^3), magnetic forces become strong enough to compete with other forces and they find this ability to recirculate flow at target locations, from this point, the maximum velocity and temperature rise linearly with increasing Mn_M. The vessel's wall porosity plays an important role in efficiency of magneto-therapy procedure because by increasing Darcy number value, the porous regions become harder and resist strongly against the blood flow passage. In this condition, the available cross sectional area for the blood flow decreases and subsequently the maximum velocity and temperature arise remarkably. As it is shown in this figure; the vessels with more rigid walls are affected later by the magnetization in view of the fact that in these cases the viscous and inertia forces are more powerful and fade the impact of magnetic forces easily as far as by tripling the wall porosity from 100 to 300, the final maximum temperature and vertical velocity at $\mathrm{Mn}_M = 5000$ drop almost 3.07 and 2.74 % respectively.

Fig. 15 shows the maximum pressure variation against magnetization number and the artery wall porosity. Maximum pressure occurs inside the porous regions corresponds to the low velocity in these locations, so by increasing Darcy number value (making the vessel's wall more rigid) the velocity magnitude in the porous media declines and as the figure depicts the maximum pressure start raising slowly. Encompassing atherosclerotic plaques in high positive pressure domain, squeezing them into the walls is one tactic in magneto-therapy procedure and base on the below figure, the maximum value of positive pressure increases severely by applying stronger external magnetic field.

Nusselt number (Nu) is an important parameter in fluid mechanic that indicates the local heat transfer rate. As was mentioned in Fig. 14, at first time steps, magnetic forces are not strong enough and only act as like as a barrier against the normal blood flow, hence as Figs. 14 and 16 indicate both blood temperature and Nusselt number value decline. After the minimum point (in this paper $\mathrm{Mn}_M = 1000$), the magnetic forces become dominant and high focused temperature enhances heat transfer rate between blood flow and atherosclerotic plaques as far as at $\mathrm{Mn}_M = 8000$, Nusselt number magnitude becomes 5 times higher than the simple case without magnetization impact. As was expected, at the present of strong external magnetic field, the value of Nu falls down respect to

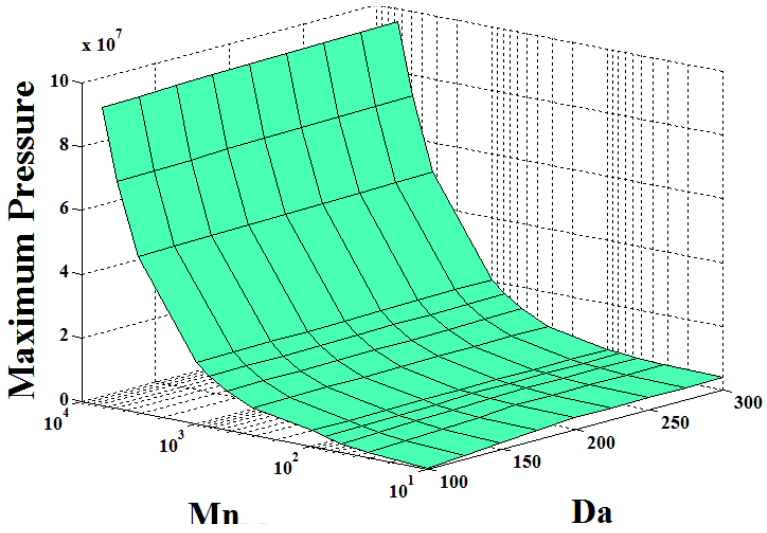

Fig. 15. Maximum pressure in different walls porosity factor and magnetization number of $\mathrm{Mn}_F = 10^7$, $\mathrm{Da}_{\mathrm{plaque}} = 500$.

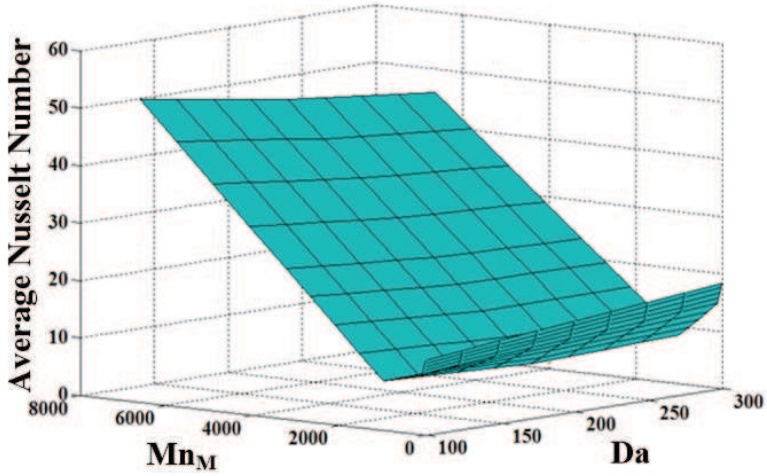

Fig. 16. Average Nusselt number in different walls porosity factor and magnetization number of $\mathrm{Mn}_F = 10^7$, $\mathrm{Da}_{\mathrm{plaque}} = 500$.

increasing the Darcy number and at $\mathrm{Mn}_M = 8000$, tripling the Darcy number reduces the Nusselt number about $10\ \%$.

The time variation of maximum viscosity and shear stress versus magnetic number are archived in Table 3. In one heart cycle, by passage of the time and slowing down the main branch inlet velocity (see Fig. 3) the maximum viscosity and shear stress go up and down respectively because the created stagnant flow produces high viscosity and low velocity gradient in the whole of vessel domain. By applying weak external magnetic field ($\mathrm{Mn}_M = 100$) although the power of viscous and inertia forces are attenuated, they remain the prevailing forces and only fluid experiences higher viscosity and lower shear stress. After $\mathrm{Mn}_M = 100$, the predominant magnetization recirculates flow and maximum viscosity and shear stress decrease and increase respectively such that at $t = 0.2$

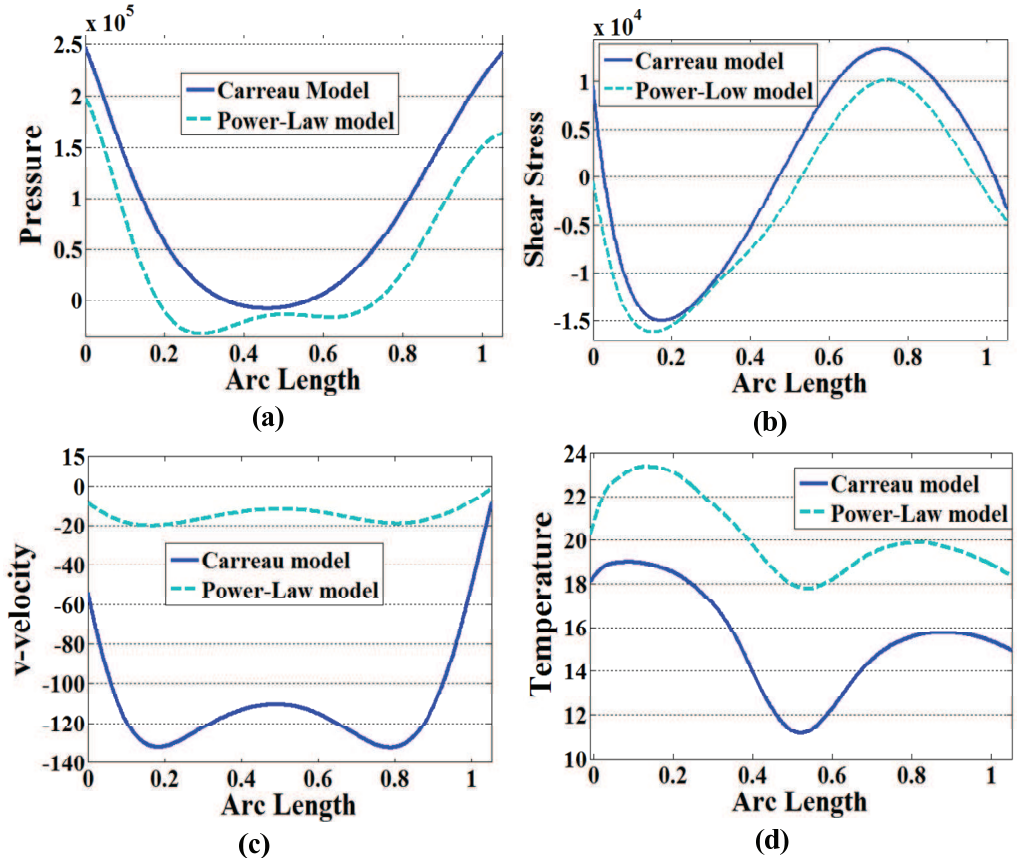

Fig. 17. Field distributions along upper plaques with two different model of non-Newtonian blood viscosity $\mathrm{Da}_{\mathrm{plaque}} = 500$, $\mathrm{Da}_{\mathrm{wall}} = 100$ and $Mn_M = 10^2$: a) pressure, b) shear stress, c) v-velocity, d) temperature.

Table 3.
Maximum viscosity and shear stress in three different time step and different magnetic field intensity with $\mathrm{Mn}_F = 0$, $\mathrm{Da}_{\mathrm{plaque}} = 500$, $\mathrm{Da}_{\mathrm{wall}} = 100$

Mn_M	Maximum Viscosity				Maximum Shear Stress			
	0.2	0.4	0.6	0.8	0.2	0.4	0.6	0.8
0	41.77	42.45	75.92	224.29	200311.39	77111.14	13819.67	4351.15
102	47.25	53.46	140.36	361.97	200115.34	77087.21	13820.75	4351.15
103	39.56	51.92	109.23	264.48	277431.85	108265.88	20492.86	6463.32
104	39.19	50.79	108.12	229.66	808842.05	313153.12	72723.71	22733.22
105	38.86	49.89	107.17	208.29	1908735.85	734105.52	218687.30	66718.63

by increasing Mn_M power two order of magnitudes (from 10^2 to 10^4), maximum viscosity drops $17.05\ \%$ while maximum shear stress becomes 4.04 times higher.

3.5. Comparison of two types of non-Newtonian viscosity models. During last decades, various mathematic formulas are suggested for modeling blood viscosity. In this part the effect of two common non-Newtonian models (power law and Carreau) on the vertical velocity, shear stress and pressure distribution through the upper and lower plaques are compared. Although the characteristics of these four parameters are approximately similar for power law and Carreau models, power law model estimates higher temperature for plaques' surfaces than the other one. This temperature increment is beneficial for magneto-therapy procedure but base on Fig. 17a, b and c power law assumption predicts lower positive pressure, fluid flux, and shear stress magnitude for atherosclerotic plaques. So, if we assume the non-Newtonian viscosity of blood and ferrofluid mixture fallows the power law formulation, analyzing the efficiency of the magnetic drug delivery procedure will face a little complicity and the priority of four parameters (temperature, pressure, shear stress, v-velocity) becomes important.

Conclusion

In this work a transient non-Newtonian blood flow in a carotid bifurcation under the influence the locally applied magnetic field is studied. Two fatty deposits atherosclerotic plaques and the vessel's walls are modeled as porous media and the numerical solution of coupled extended Navie÷- Stokes, Brinkman and energy equations are obtained by finite element method. The induced magnetic field of fixed current plates formed two vortices in the stenosis region and the value of temperature, fluid flux; shear stress and compressive pressure through the plaques' surfaces go up subsequently. From the simulation, it is observed increasing Darcy number value for both porous regions makes the magneto-therapy procedure less efficient because the maximum focused temperature and vertical velocity on plaques' surfaces decline remarkably.

REFERENCES

1. Ai, L. and Vafai, K., A Coupling Model For Macromolecule Transport in a Stenosed Arterial Wall, *Int. J. Heat Mass Transf.*, 2006, **49**, pp. 1568–1591.
2. Alexiou, C., Arnold W., Klein, R. J., Parak, F. G., Hulin, P., Bergemann, C., and Luebb, A. S., Locoregional Cancer Treatment with Magnetic Drug Targeting, *Cancer Res.*, 2000, **60**, pp. 6641–6648.
3. Alexiou, C., Jurgons, R., Schmid, R., Erhardt, W., Parak, F., Bergemann, C., and Iro H., Magnetic Drug Targeting – A New Approach in Locoregional Tumor Therapy with Chemotherapeutic Agent. Experimental animal studies, *HNO*, 2005, **53**, pp. 618–622.
4. Alimohamadi, H. and Imani, M., Computational Analysis of Synovial Fluid in Actual Three Dimensional Modeling of Human Knee Joint under the Action of Magnetic Field, *Int. J. Energy Technol.*, 2013, **4**, pp. 96–103.
5. Alimohamadi, H. and Imani, M., Transient Non-Newtonian Blood Flow under Magnetic Targeting Drug Delivery in an Aneurysm Blood Vessel with Porous Walls, *Int. J. Comput. Meth. Eng. Sci. Mech.*, 2014, **15**, pp. 522–533.
6. Asakura, T. and Karino, T., Flow Patterns and Spatial Distribution of Atherosclerotic Lesions in Human Coronary Arteries, *Circulation Res.*, 1990, **66**, pp. 1045–1066.
7. Bharadvaj, B., Mabon, R., and D. Giddens, D., Steady Flow in a Model of the Human Carotid Bifurcation. Part I. Flow Visualization, *J. Biomech.*, 1982, **15**, pp. 349–362.

8. Cho, Y. and Kensey, K., Effects of the Non-Newtonian Viscosity of Blood on Flows in a Diseased Arterial Vessel. Part 1: Steady Flows, *Biorheology*, 1990, **28**, pp. 241–262.
9. Cramer, K. R. and Pai, S.-I., *Magnetofluid Dynamics for Engineers and Applied Physicists*, McGraw-Hill, New York, 1973.
10. Duck, F. A., *Physical Properties of Tissue: A Comprehensive Reference Network*, Academic Press, London, 1990.
11. Filipović, N. D. and Kojić, M., Computer Simulations Of Blood Flow with Mass Transport through the Carotid Artery Bifurcation, *Theor. Appl. Mech.*, 2004, **31**, pp. 1–33.
12. Friedman, M. H., Hutchins, G. M., Bargeron, C. Brent, Deters,and Mark, F. F., Correlation between Intimal Thickness and Fluid Shear in Human Arteries, *Atherosclerosis*, 1981, **39**, pp. 425–436.
13. Fung, Y.-C., *Biomechanics: Circulation*, Springer, New York, 1997.
14. Giannoglou, G., Soulis, J., Farmakis, T., Farmakis, D. and Louridas, G., Haemodynamic Factors and the Important Role of Local Low Static Pressure in Coronary Wall Thickening, *Int. J. Cardiol.*, 2002, **86**, pp. 27–40.
15. Grief, A. D. and Richardson, G., Mathematical Modelling of Magnetically Targeted Drug Delivery, *J. Magnet. Magnet. Mat.*, 2005, **293**, pp. 455-463.
16. Haik, Y., Pai, V., and Chen, C.-J., Development of Magnetic Device for Cell Separation, *J. Magnet. Magnet. Mat.*, 1999, **194**, pp. 254–261.
17. Ku, D. and Liepsch, D., The Effects of Non-Newtonian Viscoelasticity and Wall Elasticity on Flow at a 90 Degrees Bifurcation, *Biorheology*, 1985, **23**, pp. 359–370.
18. Ley, O. and Kim, T., Determination of Atherosclerotic Plaque Temperature in Large Arteries, *Int. J. Thermal Sci.*, 2008, **47**, pp. 147–156.
19. Palmen, D., Gijsen, F., Vosse, V. D. F. and Janssen, J., Diagnostic Minor Stenoses in Carotid Artery Bifurcation Models Using the Disturbed Velocity Field, *J. Vasc. Investigat.*, 1997, **3**, pp. 26–41.
20. Perktold, K., Peter, R., Resch, M. and Langs, G., Pulsatile Non-Newtonian Blood Flow in Three-Dimensional Carotid Bifurcation Models: A Numerical Study of Flow Phenomena under Different Bifurcation Angles, *J. Biomed. Eng.*, 1991, **13**, pp. 507–515.
21. Perktold, K, Resch, M., and Peter, R. O., Three-Dimensional Numerical Analysis of Pulsatile Flow and Wall Shear Stress in the Carotid Artery Bifurcation, *J. Biomech.*, 1991, **24**, pp. 409–420.
22. Rathod, V. and Tanveer, S., Pulsatile Flow of Couple Stress Fluid through a Porous Medium with Periodic Body Acceleration and Magnetic Field, *Bull. Malays. Math. Sci. Soc. (2)*, 2009, **32**, pp. 245–259.
23. Scarpa, F. and Smith, F., Passive and MR Fluid-Coated Auxetic PU Foam-Mechanical, Acoustic, and Electromagnetic Properties, *J. Intel. Mat. Syst. Struct.*, 2004, **15**, pp. 973–979.
24. Schelin, A. B., Károlyi, G., de Moura, A. P., Booth, N., and Grebogi, C., Are the Fractal Skeletons the Explanation for the Narrowing of Arteries due to Cell Trapping in a Disturbed Blood Flow?, *Comput. Biol. Med.*, 2012, **42**, pp. 276–281.
25. Stangeby, D. K. and Ethier,C. R., Computational Analysis of Coupled Blood-Wall Arterial LDL Transport, *J. Biomech. Eng.*, 2002, **124**, pp. 1–8.
26. Strek, T. and Jopek, H., Computer Simulation of Heat Transfer through a Ferrofluid, *Physica Status Solidi, B*, 2007, **244**, pp. 1027–1037.
27. Sutton, G. W. and Sherman, A., *Engineering Magnetohydrodynamics*, McGraw-Hill, New York, 1965.
28. Tzirtzilakis, E., A Mathematical Model for Blood Flow in Magnetic Field, *Phys. Fluids*, 2005, **17**, pp. 077103.

29. Tzirtzilakis, E. and Loukopoulos, V., Biofluid Flow in a Channel under the Action of a Uniform Localized Magnetic Field, *Comput. Mech.*, 2005, **36**, pp. 360–374.
30. Udrea, L. E., Strachan, N J. Bădescu, V., and Rotariu, O., An Invitro Study of Magnetic Particle Targeting in Small Blood Vessels, *Phys. Med. Biol.*, 2006, **51**, pp. 48–69.
31. Wada, S. and Karino, T., Theoretical Prediction of Low-Density Lipoproteins Concentration at the Luminal Surface of an Artery with a Multiple Bend, *Annals Biomed. Eng.*, 2002, **30**, pp. 778–791.
32. Zarins, C. K., Giddens, D. P., Bharadvaj, B., Sottiurai, V. S., Mabon, R. F., and Glagov, S., Carotid Bifurcation Atherosclerosis. Quantitative Correlation of Plaque Localization with Flow Velocity Profiles and Wall Shear Stress, *Circulation Res.*, 1983, **53**, pp. 502–514.
33. Zhao, S., Xu, X., Hughes, A., Thom, S., Stanton, A., Ariff, B., and Long, Q., Blood Flow and Vessel Mechanics in a Physiologically Realistic Model of a Human Carotid Arterial Bifurcation, *J. Biomech.*, 2000, **33**, pp. 975–984.

□◆◆◆□